IEEE Access
Multidisciplinary ⋮ Rapid Review ⋮ Open Access Journal

Received November 26, 2019, accepted December 10, 2019, date of publication December 17, 2019, date of current version December 26, 2019.

Digital Object Identifier 10.1109/ACCESS.2019.2960278

Uplink Interference Management for Hetnets Stressed by Clustered Wide-Band Jammers

FAZAL MUHAMMAD[1], MUHAMMAD SAJID HAROON[2], ZIAUL HAQ ABBAS[3], GHULAM ABBAS[4], (Senior Member, IEEE), AND SUNGHWAN KIM[5]

[1]Department of Electrical Engineering, City University of Science and Information Technology, Peshawar 2500, Pakistan
[2]Telecommunications and Networking (TeleCoN) Research Lab, GIK Institute of Engineering Sciences and Technology, Topi 23640, Pakistan
[3]Faculty of Electrical Engineering, GIK Institute of Engineering Sciences and Technology, Topi 23640, Pakistan
[4]Faculty of Computer Science and Engineering, GIK Institute of Engineering Sciences and Technology, Topi 23640, Pakistan
[5]School of Electrical Engineering, University of Ulsan, Ulsan 44610, South Korea

Corresponding author: Sunghwan Kim (sungkim@ulsan.ac.kr)

This work was supported by the Research Program through the National Research Foundation of Korea under Grant NRF-2019R1A2C1005920.

ABSTRACT In heterogeneous cellular networks (HetNets), small base stations (SBSs) are overlaid in the coverage region of a macro base station (MBS) to improve coverage and spectral efficiency. However, the performance of HetNets is significantly degraded by inter-cell interference (ICI) due to aggressive frequency reuse and multi-tier deployment. Besides ICI, the uplink (UL) communications of MBS edge-users (M-EUs) are prone to jammers' interference (JI) due to wide-band jammers (WBJs). With sufficient knowledge of network parameters, such as frequency bands and transmit powers, WBJs inject JI in the UL communications band to affect legitimate communications by degrading UL signal-to-interference ratio (SIR). Such distributed denial-of-service (DDoS) attacks normally target organizations, shopping malls, or public gatherings by clustering around them. As a countermeasure, we use decoupled association (DeCA) for the M-EUs, as opposed to the coupled association (CA), to improve UL SIR. Additionally, we use proactive interference management scheme, known as reverse frequency allocation (RFA), along with DeCA to resist both ICI and JI. The results show that WBJs cluster effectively degrades the legitimate UL communications of the target. The results also demonstrate that the network performance degrades significantly by increasing jammers' density and transmit power. Furthermore, DeCA with RFA leads to improved network performance due to effective ICI and JI mitigation.

INDEX TERMS Coverage probability, denial-of-service, decoupled association, heterogeneous cellular networks, matern cluster process, poisson point process, reverse frequency allocation, wide-band jammers.

I. INTRODUCTION

A. MOTIVATION

In heterogeneous cellular networks (HetNets), coverage probability, throughput and spectrum efficiency are significantly improved by ultra-dense small base station (SBS) deployment in the macro base station (MBS) coverage area [1], [2]. With the use of orthogonal frequency division multiple access (OFDMA), there is no or limited intra-cell interference. However, inter-cell interference (ICI) is one of the main performance-limiting factors in HetNets [3], [4].

Besides ICI, uplink (UL) communication is also prone to distributed denial-of-service (DDoS) attacks due to low transmit power levels of user equipments (UEs) [5], [6]. Therefore, in this paper, we investigate wide-band jammers (WBJs) attacks to degrade UL signal-to-interference ratio (SIR) of the targets by clustering around them [7]. The WBJs' targets include organizations, shopping malls, or other public gatherings, which are assumed to be located in MBS edge area. The aim of the WBJs is to jam the UL communication as effectively as possible by injecting unwanted energy in the communication system [8], [9]. However, due to the wide-band nature of WBJs, their transmit power is limited [8]. Therefore, a sufficient number of WBJs are required to be deployed in the close proximity of the target, i.e., clustered WBJs. With the assumption that the jammers have sufficient knowledge about network parameters, such as frequency band, transmit power and target locations, WBJs create

The associate editor coordinating the review of this manuscript and approving it for publication was Young Jin Chun.

This work is licensed under a Creative Commons Attribution 4.0 License. For more information, see http://creativecommons.org/licenses/by/4.0/

coverage holes caused by jammers' interference (JI) [8], [10]. Moreover, the notion of clustered jamming is considered to be more effective as compared with uniform jamming due to a large number of jammers in the target proximity [11]. Hence, WBJs lead to substantial JI and, thus, render a target out of coverage [12].

In the state-of-the-art, HetNets have thus far followed coupled association (CA) where a UE associates with a base station (BS) both in the UL and the downlink (DL) directions under the maximum received power (MRP) association rule [13]. CA is a suitable choice when the distance between UE and the serving BS is small. However, as the distance increases, the users following CA experience more interference due to their higher UL transmit power [13]. The situation becomes worse if there exists JI. Therefore, decoupled association (DeCA) is proposed in [14], where a user associates with different tiers of BSs in UL and DL directions. UL transmit power of MBS edge users (M-EUs) significantly decreases if they associate with the nearest SBS. Hence, this leads to an improved UL SIR. Therefore, DeCA in MBS edge area is suitable for WBJs scenario, as opposed to CA that leads to severe UL interference due to high UL transmission power.

In addition to DeCA, an effective resource allocation scheme is required to further abate ICI and JI. Different resource allocation schemes have been proposed by the industry and academia to mitigate DL and UL interference, such as cell range expansion (CRE) [15], fractional frequency reuse (FFR) [16], soft frequency reuse (SFR) [17], and reverse frequency allocation (RFA) [2]. According to RFA, MBS and SBS use sub-carriers in reverse fashion for UL and DL in a multi-region environment. In this paper, we use RFA in conjunction with DeCA to effectively mitigate ICI and JI and, thus, improve UL coverage.

B. RELATED WORK

In [18], different jamming types including barrage jamming, partial-band jamming, automatic gain control jamming, equalization jamming, and synchronization jamming are studied. Moreover, various jamming attack strategies and their respective targets are presented. The authors conclude that due to the increase in the sophistication of wireless systems, more complex jamming is likely to become a bigger threat in public safety, military, and other mission-critical domains. In [19], the authors determine the presence of the jammer along with its types using deep recurrent and deep convolutional neural networks assuming OFDMA based signaling. Their results indicate that the proposed model can classify and detect jamming attacks with 85% accuracy. In [20], advanced jamming attacks in multiple-input and multiple-output (MIMO) networks are investigated, where the jammer intentionally increases the available energy to jam the target. Moreover, the authors analyze different jamming methods to compare their effectiveness in MIMO networks.

In [21] the authors use CA and DeCA to improve the experienced SIR. Their work, however, lacks any proactive interference management scheme. They characterize the coverage probability expressions for multi-tier HetNet model. The results show that DeCA outperforms CA in the proposed setup. In [22], CA and DeCA along with RFA are considered. The authors derive analytical expressions for coverage probabilities while assuming both CA and DeCA. Their results indicate that DeCA with RFA outperforms other scenarios in terms of coverage probability. Similarly, in [23], the authors investigate CA and DeCA in urban hotspots, such as shopping malls and sports stadiums. Their work considers DeCA with clustered users modeled through Matern cluster process (MCP). They derive expressions for coverage and throughput assuming both CA and DeCA. The results indicate that DeCA outperforms CA in terms of coverage and throughput. Moreover, the results show that MCP further improves the coverage and throughput of CA and DeCA.

In [24], RFA along with non-uniform HetNet (NUH) is considered. SBSs are assumed to be muted in the cell interior region and remain active in the cell edge region. Expressions for both coverage probabilities and rate coverages are derived. Results indicate that NUH with RFA shows significant improvement in rate coverages. In [25], the authors propose NUH in conjunction with SFR. They consider both uniform and nonuniform SBS distributions in the premises of MBS and analyze the effect of SFR scheme on the proposed model. Their results demonstrate that joint NUH along with SFR improves the network performance gain due to effective interference mitigation. In [26], variants of RFA are proposed with improved network performance gain. In [18]–[20], different jamming techniques are studied for both military and civil applications, however, they lack the evaluation of JI due to clustered WBJs' attack in HetNets. Therefore, in this paper, we investigate UL coverage performance of M-EUs in the presence of JI and ICI. Similarly, in [21]–[26], CA, DeCA, SFR, and RFA are used to mitigate ICI. However, in this paper, we use DeCA along with RFA to mitigate both ICI and JI.

C. APPROACH AND CONTRIBUTIONS

In this paper, a two-tier HetNet model comprising of SBSs and MBSs is considered. Moreover, WBJs are assumed to initiate attacks on the target by clustering around them. Clustered WBJs lead to severe JI with their noise energy transmission and, thus, create coverage holes. The proposed setup is depicted in Fig. 1. Moreover, MBSs, SBSs, and users are assumed to be deployed using independent homogeneous Poisson point processes (IHPPPs), while WBJs are considered to be deployed using MCP. For RFA employment, the available MBS coverage region, A_{M}, is divided into two non-overlapping regions, i.e., center region, A_{M}^{c}, and outer region, A_{M}^{o}, with radii d_1 and d_2, respectively. Similarly, SBS coverage region, A_{S}, is also divided into two non-overlapping regions, i.e., center region, A_{S}^{c}, and outer region, A_{S}^{o}, with radii x_1 and x_2, respectively (see Fig. 1).

The main contributions of this paper can be summarized as follows:

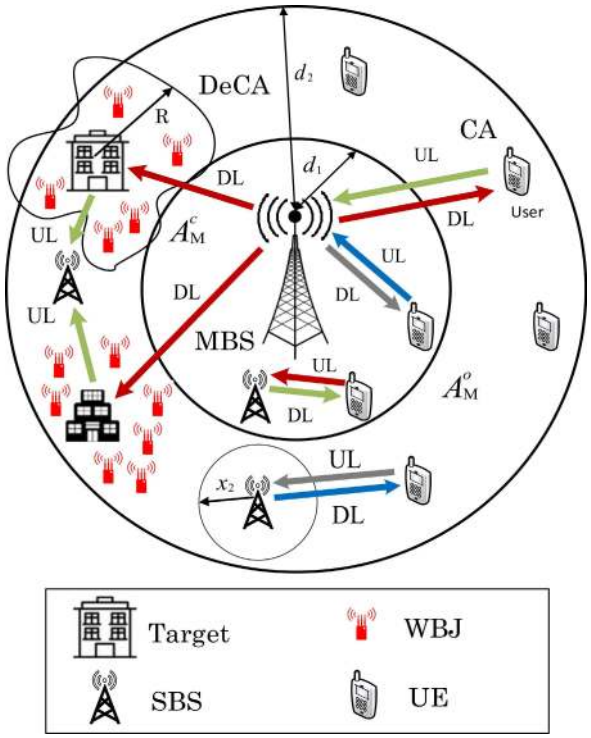

FIGURE 1. The proposed two-tier HetNet model with clustered WBJs, DeCA and RFA.

1) WBJs' cluster is assumed around the targets to create coverage holes due to JI. The targets are considered to be located in the MBS edge area and, therefore, are prone to jamming attacks due to low received SIR.
2) We investigate UL coverage of typical user[1] (ν) located in A_M^o in the presence of both ICI and JI.
3) To reduce the effect of ICI and JI, we consider DeCA along with RFA to improve UL SIR of the targets located in the MBS edge area.
4) Coverage probability expressions are derived for the following network scenarios, given that ν is located[2] in A_M^g $\forall$ $g \in (c, o)$: (i) UL coverage probability with RFA, CA, and WBJs, and (ii) UL coverage probability with RFA, DeCA, and WBJs.
5) The results are generated for various parameters, such as MBS SIR threshold, β_M, power transmitted by WBJs, $P_{t,J}$, jammers' density in the cluster, $\bar{c}$, SBS density, λ_S, UL transmitted power by ν, $P_{t,\nu}^{UL}$, and cluster radius, R.

D. PAPER ORGANIZATION

The rest of the paper is organized as follows. In Sec. II, we present the system model. In Sec. III, coverage probabilities of the proposed model are derived. Results and discussion are presented in Sec. IV. In Sec. V, the paper is concluded. The notations used in the paper are listed in Table 1.

[1] According to the Slivnyak theorem [27], a typical user at origin simplifies and retains the statistical properties of an IHPPP.

[2] Here, c and o indicate the center and outer coverage regions of MBS, respectively.

TABLE 1. Notation summary.

Notation	Description
ϕ_M, ϕ_S, ϕ_u	IHPPPs of MBSs, SBSs and users, respectively
ϕ_J	MCP of WBJs
β_M	SIR threshold for MBS
β_S	SIR threshold for SBS
d_1, d_2	Radii of A_M^c and A_M^o, respectively
$P_{t,\nu}^{UL}$	UL transmit power of ν
λ_M, λ_S	Densities of uniformly distributed MBSs and SBSs, respectively
α	Path loss exponent, $\forall$ $\alpha_M = \alpha_S = \alpha$ and $\alpha > 2$
$\lvert h \rvert$	Power gain of Rayleigh fading
r_l, r_k, r_j	distances from MBSs, SBSs, and jammers, $\forall$ $l \in \{\phi_M\}, k \in \{\phi_S\}$, and $j \in \{\phi_j\}$
SIR_M^{UL}	UL SIR received by MBS
ν	Typical user
$\bar{c}$	WBJ density
s	Laplace transform parameter
S	SBS
$''$	Coupled association
$'$	Decoupled association
η_1	Ratio of $P_{t,S}^{DL}$ and $P_{t,\nu}^{UL}$
η_2	Ratio of $P_{t,j}$ and $P_{t,\nu}^{UL}$

II. SYSTEM MODEL

This section focuses on the proposed network layout, which considers ICI due to aggressive frequency reuse and JI due to clustered WBJs attacks. In the state-of-the-art, DeCA and RFA have been shown to effectively mitigate ICI and macrocell interference (MCI) [21], [23], [28]. Therefore, as a countermeasure, we use DeCA along with RFA to mitigate JI and ICI. MBS, SBSs, and users are considered to be deployed following IHPPP while WBJs are deployed through MCP. Furthermore, mathematical preliminaries are developed in this section, which will be used for the evaluation of coverage performance in Sec. III.

A. NETWORK LAYOUT WITH ASSUMPTIONS

This paper considers a two-tier HetNet model, comprising of MBSs, SBSs, and clustered WBJs with densities λ_M, λ_S, and λ_J, respectively. MBSs, SBSs, and users are deployed through IHPPPs, i.e., ϕ_M, ϕ_S and ϕ_u, respectively, while WBJs are distributed via MCP, ϕ_J. The paper assumes a cluster of WBJs to restrict UL communication of the target by transmitting unwanted energy in the legitimate band (see Subsec. II-B for details on WBJs). More specifically, a single cluster of WBJs around the target is assumed, which causes severe JI. Therefore, only intra-cluster JI is considered, which

leads to tractable and simplified analysis. Both the WBJs and targets are assumed to be located in A_{M}^{o}. To counter both JI and ICI, in this paper, we use DeCA along with RFA (see Subsec. II-D and II-E for DeCA and RFA, respectively). The analysis is performed on ν in accordance with the Slivnyak Theorem. Moreover, ν is assumed to be located at the center of WBJs' cluster, i.e., WBJs' target. The network is considered to be interference-limited and, therefore, the effect of noise is ignored. α_{M} and α_{S} are the path loss exponents for MBS and SBS, respectively, s.t., $\alpha_{\mathrm{M}} = \alpha_{\mathrm{S}} = \alpha$. In this paper, identical path loss exponents are assumed for the sake of tractability of the numerical analysis [29], [30]. Moreover, we assume a fully loaded HetNet to simplify numerical analysis [24]. $|h|$ denotes the power gain of Rayleigh fading assumption, i.e., $|h|^2 \sim \exp(1)$.

B. WIDE-BAND JAMMERS IN HetNet

WBJs are usually defined as jammers, transmitting unwanted energy across the entire spectrum of the target [18]. WBJs stress the legitimate communications[3] through JI in order to reduce the network coverage [5], [9]. In this paper, we assume low cost and lightweight WBJ transmitters that are clustered around the target through MCP. In such a scenario, the target UL communications are affected due to (i) longer distance of users from the MBS, and (ii) severe ICI. Moreover, WBJs can be tuned to the desired HetNet communications band to make it more effective. Due to the wide-band nature of WBJs, their transmit power can be as small as of the UE' UL transmit power and can merely cause any significant damage when there are a few jammers [8]. However, as the density and power of the jammers increase, WBJs lead to sufficient JI and, thus, degrade the network performance [19].

C. SPATIAL WIDE-BAND JAMMERS MODEL

Various clustering based processes, such as the Neyman-Scott process [31], Thomas cluster process [31], and MCP [32], are studied in the state-of-the-art to model WBJs. In this paper, we use MCP due to its tractability and ease of implementation.

Definition 1 (Neyman-Scott Process): If the points per cluster with intensity $\bar{c}$ are employed using Poisson distribution, such a scenario is referred to as the Neyman-Scott process.

Definition 2 (Matern Cluster Process): MCP is a special case of Neyman-Scott process where the daughter points are distributed uniformly inside a disc of radius R *around the cluster center.*

MCP is a special case of Neyman-Scott process where the cluster centers, i.e., WBJs' targets, are modeled through parent homogeneous IHPPP $\phi_{\mathrm{T}} = \{p_0, p_1, p_2, \ldots\}$ with density λ_{T} in the Euclidean plane. Each parent point $p_i \in \{\phi_{\mathrm{T}}\}$ forms the center of the respective cluster around which daughter points, i.e., WBJs are located in the circle of radius R. Due to MCP consideration, WBJs are assumed to be modeled through uniform distribution inside R, as shown in Fig. 1. For the ease of analysis, we use $\bar{c}$ as the mean number of WBJs per cluster. Probability distribution function (PDF) for each daughter point with respect to p_i is given as

$$f(a) = \begin{cases} \dfrac{1}{\pi \mathrm{R}^2}, & ||a|| \leq \mathrm{R}, \\ 0, & \text{otherwise}. \end{cases} \tag{1}$$

Here $||a|| = r_j$ denotes the distance of an arbitrary WBJ with respect to its cluster center. In polar coordinates system, (1) can be rewritten as

$$f(r_j) = \begin{cases} \dfrac{2r_j}{\mathrm{R}^2}, & r_j \leq \mathrm{R}, \\ 0, & \text{otherwise}. \end{cases} \tag{2}$$

The resulting MCP is an isotropic and stationary point process, Ξ, with density $\bar{c}\lambda_{\mathrm{T}}$ and can be defined as $\Xi = \bigcup_{p_i \in \phi_{\mathrm{T}}} \mathcal{N}^{p_i}$, where $\mathcal{N}$ denotes the set of intra-cluster WBJs. Moreover, we perform analysis given that ν is located at the target (i.e., cluster center) under the WBJs attack.

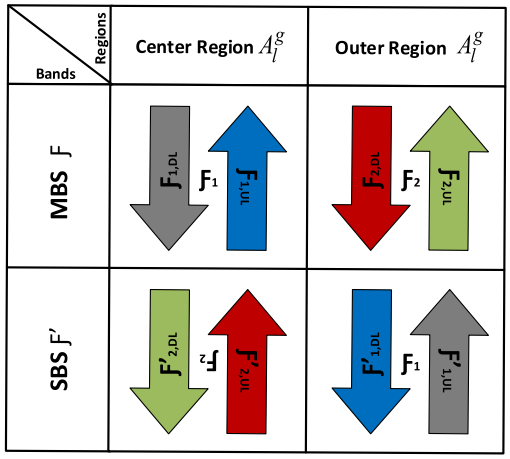

FIGURE 2. RFA model in the proposed two-tier HetNet.

D. COUPLED AND DECOUPLED ASSOCIATIONS

In CA, ν associates with the same BS of tier ω_1 both in UL and DL based on DL association rule (for the DL association rule see Definition 3) [14]. However, in DeCA, ν connects with one BS of tier ω_1 in DL based on DL association rule, and with another BS of tier ω_2 in UL following UL association rule (for the UL association rule see Definition 4). Hence, in our proposed model, ν is assumed to be associated with MBS in the DL direction from which it receives maximum power and in the UL direction with the closest SBS following path loss model.

Definition 3 (DL Association Rule): In the DL association rule, ν associates with BS of tier ω_1 based on MRP scheme [21], and the location of the serving tier ω_1 is shown as

$$\omega_1 = arg \max_{i \in (M,S)} P_{t,i}^{DL} r_{i,\nu}^{-\alpha}. \tag{3}$$

[3]Legitimate communications of both military and civil applications.

Here, $P_{t,i}^{DL}$ is the DL transmitted power from ith-tier BS *and α is the path loss exponent on the distance r.*

Definition 4 (UL Association Rule): In the UL association rule, ν associates with BS of tier ω_2 in the UL following path loss association rule, i.e., $r^{-\alpha}$ [22], and the location of the ω_2 is expressed as

$$\omega_2 = arg \max_{i\in(M,S)} r_i^{-\alpha}. \tag{4}$$

E. REVERSE FREQUENCY ALLOCATION

In HetNets, aggressive frequency reuse is employed to obtain high throughput. This, however, leads to higher ICI. Spectral efficiency[4] is improved by using separate sub-bands for both UL and DL transmissions. Therefore, in our proposed model, we use RFA to mitigate interference and increase spectral efficiency. In RFA, different sub-bands between SBSs and MBSs are used in A_l^g $\forall$ $g \in (c, o)$ and $l \in$ (M, S) in a complementary fashion, as shown in Fig. 2.

In Fig. 2, according to RFA, the total allocated bandwidth, $\mathcal{F}$, is divided into two sub-bands, i.e., $\mathcal{F}_1$ and $\mathcal{F}_2$, such that $\mathcal{F} = \bigcup_{z\in(1,2)} \mathcal{F}_z$. Here, $\mathcal{F}_1$ and $\mathcal{F}_2$ denote the sub-bands of MBS to be used in A_{M}^o and A_{M}^c, respectively, and vice versa. Sub-bands $\mathcal{F}_1$ and $\mathcal{F}_2$ are further divided into UL and DL sub-carriers and are modeled as $\mathcal{F}_1 = \mathcal{F}_{1,\mathrm{UL}} + \mathcal{F}_{1,\mathrm{DL}}$ and $\mathcal{F}_2 = \mathcal{F}_{2,\mathrm{UL}} + \mathcal{F}_{2,\mathrm{DL}}$, respectively. The sub-bands, $\mathcal{F}_1$ and $\mathcal{F}_2$, of the MBS are used as the frequency sub-bands, $\mathcal{F}_1'$ and $\mathcal{F}_2'$, for the SBSs but in reverse directions with corresponding alternate regions, i.e., SBS outer region, A_{S}^o, and SBS center region, A_{S}^c, respectively. The bands, $\mathcal{F}_1'$ and $\mathcal{F}_2'$, for SBSs are further divided into UL and DL sub-carriers and are given as $\mathcal{F}_2' = \mathcal{F}_{2,\mathrm{UL}}' + \mathcal{F}_{2,\mathrm{DL}}'$ and $\mathcal{F}_1' = \mathcal{F}_{1,\mathrm{UL}}' + \mathcal{F}_{1,\mathrm{DL}}'$, respectively. RFA based resource partitioning not only enhances the coverage but also reduces interference as there is no dedicated spectrum allocated for SBS transmission. Thus, by employing RFA, the whole MBS spectrum is made available to SBSs but in reverse directions and in alternate regions.

III. ANALYSIS OF COVERAGE PROBABILITY

In this section, expressions for coverage probabilities are derived for the following network scenarios, given that ν is located in A_{M}^c and in A_{M}^o: (i) UL coverage probability for ν with RFA, CA, and WBJs (see Subsection III-A), and (ii) UL coverage probability for ν with RFA, DeCA, and WBJs (see Subsection III-B).

A. UPLINK COVERAGE PROBABILITY WITH COUPLED ASSOCIATION

1) UL COVERAGE PROBABILITY GIVEN THAT ν IS LOCATED IN A_{M}^C with RFA, CA, and WBJs

UL coverage probability expression for ν in A_{M}^c with RFA, CA, and WBJs, i.e., $P_{A_{\mathrm{M}}^c}^{\mathrm{UL}''}(\beta_{\mathrm{M}})$, and can be written as

$$P_{A_{\mathrm{M}}^c}^{\mathrm{UL}''}(\beta_{\mathrm{M}}) = P\left(\mathrm{SIR}_{\mathrm{M}}^{\mathrm{UL}} > \beta_{\mathrm{M}}\right). \tag{5}$$

[4]Information transmission rate over a given bandwidth.

Here, β_{M} is the MBS association SIR threshold. Due to RFA employment, the received UL interference is the sum of UL interference from the MBS-tier in A_{M}^c, i.e., $I_{\phi_{\mathrm{M}},A_{\mathrm{M}}^c}^{\mathrm{UL}}$, DL interference from the SBS-tier in A_{M}^o, i.e., $I_{\phi_{\mathrm{S}},A_{\mathrm{M}}^o}^{\mathrm{DL}}$, and interference from jammers in A_{M}^o, i.e., $I_{\phi_J,A_{\mathrm{M}}^o}$. Therefore, $\mathrm{SIR}_{\mathrm{M}}^{\mathrm{UL}}$ in (5) can be written as

$$\mathrm{SIR}_{\mathrm{M}}^{\mathrm{UL}} = \frac{P_{t,\nu}^{\mathrm{UL}}|h_{\mathrm{M}}|r_{\mathrm{M}}^{-\alpha}}{I_{\phi_{\mathrm{M}},A_{\mathrm{M}}^c}^{\mathrm{UL}} + I_{\phi_{\mathrm{S}},A_{\mathrm{M}}^o}^{\mathrm{DL}} + I_{\phi_J,A_{\mathrm{M}}^o}}. \tag{6}$$

Eq. (6) can be further expanded as

$$\mathrm{SIR}_{\mathrm{M}}^{\mathrm{UL}} = \frac{P_{t,\nu}^{\mathrm{UL}}|h_{\mathrm{M}}|r_{\mathrm{M}}^{-\alpha}}{\sum_{l\in\phi_{\mathrm{M}}} P_{t,l}^{\mathrm{UL}}|h_l|r_l^{-\alpha} + \sum_{k\in\phi_{\mathrm{S}}} P_{t,k}^{\mathrm{DL}}|h_k|^2 r_k^{-\alpha} + \sum_{j\in\phi_J} P_{t,j}|h_l|r_j^{-\alpha}}. \tag{7}$$

Here, $P_{t,\nu}^{\mathrm{UL}}$ is the UL transmit power of ν, $P_{t,l}^{\mathrm{UL}}$ is the UL transmit power of MBS, and $P_{t,k}^{\mathrm{DL}}$ is the DL transmit power of SBS. By substituting (6) into (5), $P_{A_{\mathrm{M}}^c}^{\mathrm{UL}''}(\beta_{\mathrm{M}})$ is written as

$$\begin{aligned}
&P_{A_{\mathrm{M}}^c}^{\mathrm{UL}''}(\beta_{\mathrm{M}}) \\
&\overset{(1)}{=} P\left(\frac{P_{t,\nu}^{\mathrm{UL}}|h_{\mathrm{M}}|r_{\mathrm{M}}^{-\alpha}}{I_{\phi_{\mathrm{M}},A_{\mathrm{M}}^c}^{\mathrm{UL}} + I_{\phi_{\mathrm{S}},A_{\mathrm{M}}^o}^{\mathrm{DL}} + I_{\phi_J,A_{\mathrm{M}}^o}} > \beta_{\mathrm{M}}\right) \\
&\overset{(2)}{=} \mathrm{E}_{r_{\mathrm{M}},I_{\phi_{\mathrm{M}},A_{\mathrm{M}}^c}^{\mathrm{UL}},I_{\phi_{\mathrm{S}},A_{\mathrm{M}}^o}^{\mathrm{DL}},I_{\phi_J,A_{\mathrm{M}}^o}} \\
&\quad\times\left[\exp\left(-\frac{r_{\mathrm{M}}^{\alpha}\beta_{\mathrm{M}}}{P_{t,\nu}^{\mathrm{UL}}}\left(I_{\phi_{\mathrm{M}},A_{\mathrm{M}}^c}^{\mathrm{UL}} + I_{\phi_{\mathrm{S}},A_{\mathrm{M}}^o}^{\mathrm{DL}} + I_{\phi_J,A_{\mathrm{M}}^o}\right)\right)\right] \\
&\overset{(3)}{=} \mathrm{E}_{r_{\mathrm{M}},I_{\phi_{\mathrm{M}},A_{\mathrm{M}}^c}^{\mathrm{UL}},I_{\phi_{\mathrm{S}},A_{\mathrm{M}}^o}^{\mathrm{DL}},I_{\phi_J,A_{\mathrm{M}}^o}} \\
&\quad\times\left[\exp\left(-s\left(I_{\phi_{\mathrm{M}},A_{\mathrm{M}}^c}^{\mathrm{UL}} + I_{\phi_{\mathrm{S}},A_{\mathrm{M}}^o}^{\mathrm{DL}} + I_{\phi_J,A_{\mathrm{M}}^o}\right)\right)\right] \\
&\overset{(4)}{=} \mathrm{E}_{r_{\mathrm{M}}}\left[\mathrm{E}_{I_{\phi_{\mathrm{M}},A_{\mathrm{M}}^c}^{\mathrm{UL}}}\exp\left(-s\left(I_{\phi_{\mathrm{M}},A_{\mathrm{M}}^c}^{\mathrm{UL}}\right)\right)\right. \\
&\quad\times\mathrm{E}_{I_{\phi_{\mathrm{S}},A_{\mathrm{M}}^o}^{\mathrm{DL}}}\exp\left(-s\left(I_{\phi_{\mathrm{S}},A_{\mathrm{M}}^o}^{\mathrm{DL}}\right)\right) \\
&\quad\left.\times\mathrm{E}_{I_{\phi_J,A_{\mathrm{M}}^o}}\exp\left(-s\left(I_{\phi_J,A_{\mathrm{M}}^o}\right)\right)\right] \\
&\overset{(5)}{=} \mathrm{E}_{r_{\mathrm{M}}}\left[\mathcal{L}_{I_{\phi_{\mathrm{M}},A_{\mathrm{M}}^c}^{\mathrm{UL}}}(s)\times\mathcal{L}_{I_{\phi_{\mathrm{S}},A_{\mathrm{M}}^o}^{\mathrm{DL}}}(s)\times\mathcal{L}_{I_{\phi_J,A_{\mathrm{M}}^o}}(s)\right].
\end{aligned} \tag{8}$$

Here, Step (1) is obtained from the definition of coverage probability [2], [27]. Step (2) is obtained from Step (1) (see Appendix for the proof of Step (2)). Similarly, Step (3) is obtained by replacing $\frac{r_{\mathrm{M}}^{\alpha}\beta_{\mathrm{M}}}{P_{t,\nu}^{\mathrm{UL}}}$ by s, where $s = \frac{r_{\mathrm{M}}^{\alpha}\beta_{\mathrm{M}}}{P_{t,\nu}^{\mathrm{UL}}}$. Moreover, Step (4) is obtained by using the exponential property of sums into products, i.e., $\exp(a+b) = \exp(a)\times\exp(b)$. Finally, Step (5) is obtained from Step (4) by using the definition of Laplace transform (see (2.12) of [27]).

The Laplace transform of the UL interference from the MBS-tier in A_{M}^{c}, i.e., $\mathcal{L}_{I^{\mathrm{UL}}_{\phi_{\mathrm{M}},A_{\mathrm{M}}^{c}}}(s)$ is obtained as

$$\begin{aligned}
&\mathcal{L}_{I^{\mathrm{UL}}_{\phi_{\mathrm{M}},A_{\mathrm{M}}^{c}}}(s)\\
&\overset{(a)}{=} \mathrm{E}_{I^{\mathrm{UL}}_{\phi_{\mathrm{M}},A_{\mathrm{M}}^{c}}}\left[\exp\left(-I^{\mathrm{UL}}_{\phi_{\mathrm{M}},A_{\mathrm{M}}^{c}}s\right)\right]\Bigg|_{s=\frac{r_{\mathrm{M}}^{\alpha}\beta_{\mathrm{M}}}{P^{\mathrm{UL}}_{t,\nu}}}\\
&\overset{(b)}{=} \mathrm{E}_{I^{\mathrm{UL}}_{\phi_{\mathrm{M}},A_{\mathrm{M}}^{c}},|h_l|}\left[\exp\left(-s\sum_{j\in\phi_{\mathrm{M}}}P^{\mathrm{UL}}_{t,\nu}|h_l|r_l^{-\alpha}\right)\right]\\
&\overset{(c)}{=} \mathrm{E}_{I^{\mathrm{UL}}_{\phi_{\mathrm{M}},A_{\mathrm{M}}^{c}},|h_l|}\left[\prod_{l\in\phi_{\mathrm{M}}}\exp\left(-|h_l|\beta_{\mathrm{M}}r_{\mathrm{M}}^{\alpha}r_l^{-\alpha}\right)\right]\\
&\overset{(d)}{=} \mathrm{E}_{I^{\mathrm{UL}}_{\phi_{\mathrm{M}},A_{\mathrm{M}}^{c}},|h_l|}\left[\prod_{l\in\phi_{\mathrm{M}}}\mathrm{E}_{|h_l|}\exp\left(-|h_l|\beta_{\mathrm{M}}r_{\mathrm{M}}^{\alpha}r_l^{-\alpha}\right)\right]\\
&\overset{(e)}{=} \mathrm{E}_{I^{\mathrm{UL}}_{\phi_{\mathrm{M}},A_{\mathrm{M}}^{c}}}\left[\prod_{l\in\phi_{\mathrm{M}}}\frac{1}{1+\beta_{\mathrm{M}}\left(\frac{r_l}{r_{\mathrm{M}}}\right)^{-\alpha}}\right]\\
&\overset{(f)}{=} \exp\left(-2\pi\lambda_{\mathrm{M}}\int_{y}^{d_1}\frac{r_l dr_l}{1+\left(\frac{r_l}{\beta_{\mathrm{M}}^{1/\alpha}r_{\mathrm{M}}}\right)^{\alpha}}\right)\\
&\overset{(g)}{=} \exp\left(-\pi\lambda_{\mathrm{M}}\beta_{\mathrm{M}}^{2/\alpha}r_{\mathrm{M}}^{2}\int_{\left(\frac{y}{\beta_{\mathrm{M}}^{1/\alpha}r_{\mathrm{M}}}\right)^{2}}^{\left(\frac{d_1}{\beta_{\mathrm{M}}^{1/\alpha}r_{\mathrm{M}}}\right)^{2}}\frac{du}{1+(u)^{\alpha/2}}\right)\\
&\overset{(h)}{=} \exp\Bigg(\frac{\lambda_{\mathrm{M}}\pi\beta_{\mathrm{M}}d_1^{(2-\alpha)}r_{\mathrm{M}}^{\alpha}}{\alpha/2-1}{}_2F_1\\
&\quad\times\left(1,1-\frac{2}{\alpha},2-\frac{2}{\alpha},-\beta_{\mathrm{M}}\left(\frac{r_{\mathrm{M}}}{d_1}\right)^{\alpha}\right)\\
&\quad-\frac{\lambda_{\mathrm{M}}\pi\beta_{\mathrm{M}}y^{(2-\alpha)}r_{\mathrm{M}}^{\alpha}}{\alpha/2-1}{}_2F_1\\
&\quad\times\left(1,1-\frac{2}{\alpha},2-\frac{2}{\alpha},-\beta_{\mathrm{M}}\left(\frac{r_{\mathrm{M}}}{y}\right)^{\alpha}\right)\Bigg). \qquad (9)
\end{aligned}$$

Here, Step (a) is obtained from the definition of Laplace transform [27], Step (b) is obtained by substituting the value of $I^{\mathrm{UL}}_{\phi_{\mathrm{M}},A_{\mathrm{M}}^{c}}=\sum_{l\in\phi_{\mathrm{M}}}P^{\mathrm{UL}}_{t,l}|h_l|r_l^{-\alpha}$, into Step (a), Step (c) is obtained by substituting the value of s, s.t., $s=\frac{r_{\mathrm{M}}^{\alpha}\beta_{\mathrm{M}}}{P^{\mathrm{UL}}_{t,\nu}}$, into Step (b), Step (e) is obtained by computing the Laplace transform of Step (d) with respect to h_j, Step (f), is obtained by using probability generating functional (PGFL) of IHPPP [33], Step (g) is obtained by substituting $u=\left(\frac{r_j}{(\beta_{\mathrm{M}})^{1/\alpha}r_{\mathrm{M}}}\right)^2$ into Step (f), and Step (h) is obtained by Gauss-hypergeometric approximation of Step (g) [33].

Similarly, the Laplace transform of the received UL interference from the MBS-tier in A_{M}^{o}, i.e., $\mathcal{L}_{I^{\mathrm{UL}}_{\phi_{\mathrm{M}},A_{\mathrm{M}}^{o}}}(s)$, is obtained as

$$\begin{aligned}
\mathcal{L}_{I^{\mathrm{UL}}_{\phi_{\mathrm{M}},A_{\mathrm{M}}^{o}}}(s) = \exp\Bigg(&\frac{\lambda_{\mathrm{M}}\pi\beta_{\mathrm{M}}d_2^{(2-\alpha)}r_{\mathrm{M}}^{\alpha}}{\alpha/2-1}{}_2F_1\\
&\times\left(1,1-\frac{2}{\alpha},2-\frac{2}{\alpha},-\beta_{\mathrm{M}}\left(\frac{r_{\mathrm{M}}}{d_2}\right)^{\alpha}\right)\\
&-\frac{\lambda_{\mathrm{M}}\pi\beta_{\mathrm{M}}d_1^{(2-\alpha)}r_{\mathrm{M}}^{\alpha}}{\alpha/2-1}{}_2F_1\\
&\times\left(1,1-\frac{2}{\alpha},2-\frac{2}{\alpha},-\beta_{\mathrm{M}}\left(\frac{r_{\mathrm{M}}}{d_1}\right)^{\alpha}\right)\Bigg). \qquad (10)
\end{aligned}$$

Moreover, the Laplace transform of the DL interference from the SBS-tier in A_{M}^{o}, i.e., $\mathcal{L}_{I^{\mathrm{DL}}_{\phi_{\mathrm{S}},A_{\mathrm{M}}^{c}}}$, is obtained in a similar way as for (9) and is written as

$$\begin{aligned}
\mathcal{L}_{I^{\mathrm{DL}}_{\phi_{\mathrm{S}},A_{\mathrm{M}}^{c}}} &= \mathcal{L}_{I^{\mathrm{DL}}_{\phi_{\mathrm{S}},A_{\mathrm{M}}^{o}}}\\
&= \exp\Bigg(\frac{\lambda_{\mathrm{S}}\pi\eta_1\beta_{\mathrm{M}}x_2^{(2-\alpha)}r_{\mathrm{M}}^{\alpha}}{\alpha/2-1}{}_2F_1\\
&\quad\times\left(1,1-\frac{2}{\alpha},2-\frac{2}{\alpha},-\eta_1\beta_{\mathrm{M}}\left(\frac{r_{\mathrm{M}}}{x_2}\right)^{\alpha}\right)\\
&\quad-\frac{\lambda_{\mathrm{S}}\pi\eta_1\beta_{\mathrm{M}}x_1^{(2-\alpha)}r_{\mathrm{M}}^{\alpha}}{\alpha/2-1}{}_2F_1\\
&\quad\times\left(1,1-\frac{2}{\alpha},2-\frac{2}{\alpha},-\eta_1\beta_{\mathrm{M}}\left(\frac{r_{\mathrm{M}}}{x_1}\right)^{\alpha}\right)\Bigg). \qquad (11)
\end{aligned}$$

Here, non-italic and uppercase S denotes SBS while italic and lowercase s indicates the Laplace transform parameter. Moreover, $\eta_1=\frac{P^{\mathrm{DL}}_{t,\mathrm{S}}}{P^{\mathrm{UL}}_{t,\nu}}$, where $P^{\mathrm{DL}}_{t,\mathrm{S}}$ is the DL transmit power of SBSs.

Similarly, from (11), the Laplace transform of the UL interference from the SBS-tier in A_{M}^{o}, i.e., $\mathcal{L}_{I^{\mathrm{UL}}_{\phi_{\mathrm{S}},A_{\mathrm{M}}^{o}}}$, can be obtained as

$$\begin{aligned}
\mathcal{L}_{I^{\mathrm{UL}}_{\phi_{\mathrm{S}},A_{\mathrm{M}}^{o}}} = \nu\exp\Bigg(&\frac{\lambda_{\mathrm{S}}\pi\beta_{\mathrm{M}}x_2^{(2-\alpha)}r_{\mathrm{M}}^{\alpha}}{\alpha/2-1}{}_2F_1\\
&\times\left(1,1-\frac{2}{\alpha},2-\frac{2}{\alpha},-\beta_{\mathrm{M}}\left(\frac{r_{\mathrm{M}}}{x_2}\right)^{\alpha}\right)\\
&-\frac{\lambda_{\mathrm{S}}\pi\beta_{\mathrm{M}}x_1^{(2-\alpha)}r_{\mathrm{M}}^{\alpha}}{\alpha/2-1}{}_2F_1\\
&\times\left(1,1-\frac{2}{\alpha},2-\frac{2}{\alpha},-\beta_{\mathrm{M}}\left(\frac{r_{\mathrm{M}}}{x_1}\right)^{\alpha}\right)\Bigg). \qquad (12)
\end{aligned}$$

The Laplace transform of interference received from jammer's cluster in A_{M}^{o}, i.e., $\mathcal{L}'_{I_{\phi_J,A_{\mathrm{M}}^{o}}}$, while assuming that ν is associated with the MBS following CA, can be obtained as

$$\mathcal{L}'_{I_{\phi_J,A_{\mathrm{M}}^{o}}} \overset{(i)}{=} \mathrm{E}_{I_{\mathrm{M},A_{\mathrm{M}}^{o}}}\left[\exp\left(-sI_{\phi_J,A_{\mathrm{M}}^{o}}\right)\right]\Bigg|_{s=\frac{r_{\mathrm{M}}^{\alpha}\beta_{\mathrm{M}}}{P^{\mathrm{UL}}_{t,\nu}}}$$

$$\overset{(j)}{=} \mathrm{E}_{I'_{\phi_J,A_{\mathrm{M}}^o},|h_l|}\left[\exp\left(-s\sum_{j\in\phi_J}P_{t,J}|h_l|r_j^{-\alpha}\right)\right]$$

$$\overset{(k)}{=} \mathrm{E}_{I'_{\phi_J,A_{\mathrm{M}}^o},|h_l|}\left[\prod_{j\in\phi_J}\exp\left(-|h_l|\eta_2\beta_{\mathrm{M}}r_{\mathrm{M}}^{\alpha}r_j^{-\alpha}\right)\right]$$

$$\overset{(l)}{=} \mathrm{E}_{I'_{\phi_J,A_{\mathrm{M}}^o}}\left[\prod_{j\in\phi_J}\mathrm{E}_{|h_l|}\exp\left(-|h_l|\eta_2\beta_{\mathrm{M}}r_{\mathrm{M}}^{\alpha}r_j^{-\alpha}\right)\right]$$

$$\overset{(m)}{=} \mathrm{E}_{I'_{\phi_J,A_{\mathrm{M}}^o}}\left[\prod_{j\in\phi_J}\frac{1}{1+\eta_2\beta_{\mathrm{M}}\left(\frac{r_j}{r_{\mathrm{M}}}\right)^{-\alpha}}\right]$$

$$\overset{(n)}{=} \exp\left(-\bar{c}\int_z^{\mathrm{R}}\left(\frac{f(r_j)dr_j}{1+\eta_2\beta_{\mathrm{M}}\left(\frac{r_j}{r_{\mathrm{M}}}\right)^{-\alpha}}\right)\right)$$

$$\overset{(o)}{=} \exp\left(-\bar{c}\int_z^{\mathrm{R}}\frac{2r_jdr_j}{\mathrm{R}^2\left(1+\eta_2\beta_{\mathrm{M}}\left(\frac{r_j}{r_{\mathrm{M}}}\right)^{-\alpha}\right)}\right)$$

$$\overset{(p)}{=} \exp\Bigg[-\bar{c}\Bigg(\frac{2\mathrm{R}^{2+\alpha}r_{\mathrm{M}}^{-\alpha}}{\mathrm{R}^2(2+\alpha)\beta_{\mathrm{M}}\eta_2}{}_2F_1\left(1,1+\frac{2}{\alpha},2+\frac{2}{\alpha},-\left(\frac{\mathrm{R}^{\alpha}}{r_{\mathrm{M}}^{\alpha}\beta_{\mathrm{M}}\eta_2}\right)\right)-\frac{2z^{2+\alpha}r_{\mathrm{M}}^{-\alpha}}{z^2(2+\alpha)\beta_{\mathrm{M}}\eta_2}{}_2F_1\times\left(1,1+\frac{2}{\alpha},2+\frac{2}{\alpha},-\left(\frac{z^{\alpha}}{r_{\mathrm{M}}^{\alpha}\beta_{\mathrm{M}}\eta_2}\right)\right)\Bigg)\Bigg]. \quad (13)$$

Here, Step (i) is obtained from the definition of Laplace transform [27], Step (j) is obtained by substituting the value of $I_{\phi_J,A_{\mathrm{M}}^o}=\sum_{j\in\phi_J}P_{t,j}|h_j|r_j^{-\alpha}$ into Step (i), Step (k) is obtained by substituting the value of s, s.t., $s=\frac{r_{\mathrm{M}}^{\alpha}\beta_{\mathrm{M}}}{P_{t,\nu}^{\mathrm{UL}}}$ into Step (j), Step (m) is obtained by computing the Laplace transform of Step (l) with respect to h_j, Step (n) is obtained by considering MCP intra-cluster interference for single cluster [34], [35], Step (o) is obtained by substituting the value of $f(r_j)$ in Step (n), Step (p) is obtained by taking Gauss-hypergeometric approximation of Step (o), and η_2 denotes the ratio $\frac{P_{t,J}}{P_{t,\nu}^{\mathrm{UL}}}$.

The Laplace transform of interference received from jammer's cluster in A_{M}^o, i.e., $\mathcal{L}_{I_{\phi_J,A_{\mathrm{M}}^o}}$, while assuming that ν is associated with the SBS through DeCA, can be obtained as

$$\mathcal{L}_{I_{\phi_J,A_{\mathrm{M}}^o}} = \exp\Bigg[-\bar{c}\Bigg(\frac{2\mathrm{R}^{2+\alpha}r_{\mathrm{S}}^{-\alpha}}{\mathrm{R}^2(2+\alpha)\beta_{\mathrm{S}}\eta_2}{}_2F_1\times\left(1,1+\frac{2}{\alpha},2+\frac{2}{\alpha},-\left(\frac{\mathrm{R}^{\alpha}}{r_{\mathrm{S}}^{\alpha}\beta_{\mathrm{S}}\eta_2}\right)\right)-\frac{2z^{2+\alpha}r_{\mathrm{S}}^{-\alpha}}{z^2(2+\alpha)\beta_{\mathrm{S}}\eta_2}{}_2F_1\left(1,1+\frac{2}{\alpha},2+\frac{2}{\alpha},-\left(\frac{z^{\alpha}}{r_{\mathrm{S}}^{\alpha}\beta_{\mathrm{S}}\eta_2}\right)\right)\Bigg)\Bigg]. \quad (14)$$

Moreover, assuming that ν is located in both A_{M}^c, i.e., $\nu_{A_{\mathrm{M}}^c}$ while associated with the MBS at a distance r_{M} has PDFs, given as [27]

$$f_{r_{\mathrm{M}}|\nu_{A_{\mathrm{M}}^c}}(r_{\mathrm{M}})=\frac{2\pi\lambda_{\mathrm{M}}r_{\mathrm{M}}\exp(-\lambda_{\mathrm{M}}\pi r_{\mathrm{M}}^2)}{1-\exp\left(-\lambda_{\mathrm{M}}\pi d_1^2\right)}, \quad (15)$$

and assuming that ν is located in A_{M}^o, i.e., $\nu_{A_{\mathrm{M}}^o}$ while associated with the MBS at a distance r_{M} has PDFs, given as [27]

$$f_{r_{\mathrm{M}}|\nu_{A_{\mathrm{M}}^o}}(r_{\mathrm{M}})=\frac{2\pi\lambda_{\mathrm{M}}r_{\mathrm{M}}\exp(-\lambda_{\mathrm{M}}\pi r_{\mathrm{M}}^2)}{\exp\left(-\lambda_{\mathrm{M}}\pi d_1^2\right)}. \quad (16)$$

Similarly, assuming that ν is located in A_{S}^c, i.e., $\nu_{A_{\mathrm{S}}^c}$ while associated with the SBS at a distance r_{S} has PDFs, given as

$$f_{r_{\mathrm{S}}|\nu_{A_{\mathrm{S}}^c}}(r_{\mathrm{S}})=\frac{2\pi\lambda_{\mathrm{S}}r_{\mathrm{S}}\exp(-\lambda_{\mathrm{S}}\pi r_{\mathrm{S}}^2)}{1-\exp\left(-\lambda_{\mathrm{M}}\pi d_1^2\right)}, \quad (17)$$

and assuming that ν is located in in A_{S}^o, i.e., $\nu_{A_{\mathrm{S}}^o}$, while associated with the SBS at a distance r_{S} has PDFs, given as

$$f_{r_{\mathrm{S}}|\nu_{A_{\mathrm{S}}^o}}(r_{\mathrm{S}})=\frac{2\pi\lambda_{\mathrm{S}}r_{\mathrm{S}}\exp(-\lambda_{\mathrm{S}}\pi r_{\mathrm{S}}^2)}{\exp\left(-\lambda_{\mathrm{M}}\pi d_1^2\right)}. \quad (18)$$

UL coverage probability expression, $P_{A_{\mathrm{M}}^c}^{\mathrm{UL}''}(\beta_{\mathrm{M}})$, for MBS associated ν in A_{M}^c with RFA, CA, and WBJs can be written as [3]

$$P_{A_{\mathrm{M}}^c}^{\mathrm{UL}''}(\beta_{\mathrm{M}})=\int_y^{d_1}\left[\mathcal{L}_{I_{\phi_{\mathrm{M}},A_{\mathrm{M}}^c}^{\mathrm{UL}}}(s)\times\mathcal{L}_{I_{\phi_{\mathrm{S}},A_{\mathrm{M}}^o}^{\mathrm{DL}}}(s)\times\mathcal{L}'_{I_{\phi_J,A_{\mathrm{M}}^o}}(s)\right]\times f_{r_{\mathrm{M},\nu}|\nu_{A_{\mathrm{M}}^c}}(r_{\mathrm{M},\nu})\,dr_{\mathrm{M},\nu}. \quad (19)$$

By substituting (9), (11), (13) and (15) into (19), $P_{A_{\mathrm{M}}^c}^{\mathrm{UL}''}(\beta_{\mathrm{M}})$ can be written in (21), as shown at the bottom of next page.

2) UL COVERAGE PROBABILITY GIVEN THAT ν IS LOCATED IN A_{M}^O WITH RFA, CA, AND WBJs

UL coverage probability expression for ν in A_{M}^o with RFA, CA, and WBJs, i.e., $P_{A_{\mathrm{M}}^o}^{\mathrm{UL}''}(\beta_{\mathrm{M}})$, can be obtained as

$$P_{A_{\mathrm{M}}^o}^{\mathrm{UL}''}(\beta_{\mathrm{M}})=\int_{d_1}^{d_2}\mathcal{L}_{I_{\phi_{\mathrm{M}},A_{\mathrm{M}}^o}^{\mathrm{UL}}}(s)\times\mathcal{L}_{I_{\phi_{\mathrm{S}},A_{\mathrm{M}}^c}^{\mathrm{DL}}}(s)\times\mathcal{L}'_{I_{\phi_J,A_{\mathrm{M}}^o}}(s)\times f_{r_{\mathrm{M},\nu}|\nu_{A_{\mathrm{M}}^o}}(r_{\mathrm{M},\nu})\,dr_{\mathrm{M},\nu}. \quad (20)$$

By substituting (10), (11), (13) and (16) into (20), $P_{A_{\mathrm{M}}^o}^{\mathrm{UL}''}(\beta_{\mathrm{M}})$ can be written in (22), as shown at the bottom of next page.

B. UPLINK COVERAGE PROBABILITY WITH DECOUPLED ASSOCIATION

1) UL COVERAGE PROBABILITY GIVEN THAT ν IS LOCATED IN A_{M}^C WITH RFA, DeCA, AND WBJs

In the proposed model, DeCA is not considered in A_{M}^c. Therefore, the UL coverage probability expression for ν in A_{M}^c

with RFA, CA, and WBJs is the same as the UL coverage probability expression for ν in A_{M}^{c} with RFA, DeCA, and WBJs, i.e, $P_{A_{\mathrm{M}}^{c}}^{\mathrm{UL}''}(\beta_{\mathrm{M}}) = P_{A_{\mathrm{M}}^{c}}^{\mathrm{UL}'}(\beta_{\mathrm{M}})$ (given by (21)).

2) UL COVERAGE PROBABILITY GIVEN THAT ν IS LOCATED IN A_{M}^{O} WITH RFA, DeCA, AND WBJs

From (20), UL coverage probability expression for ν in A_{M}^{o} with RFA, DeCA, and WBJs, i.e., $P_{A_{\mathrm{M}}^{o}}^{\mathrm{UL}'}(\beta_{\mathrm{M}})$, can be rewritten as

$$P_{A_{\mathrm{M}}^{o}}^{\mathrm{UL}'}(\beta_{\mathrm{S}}) = \int_{d_1}^{d_2} \left[\mathcal{L}_{I_{\phi_{\mathrm{S}},A_{\mathrm{M}}^{o}}^{\mathrm{UL}}}(s) \times \mathcal{L}_{I_{\phi_{\mathrm{S}},A_{\mathrm{M}}^{c}}^{\mathrm{DL}}}(s) \times \mathcal{L}_{I_{\phi_J,A_{\mathrm{M}}^{o}}}(s)\right] \times f_{r_{\mathrm{S}}|U_{A_{\mathrm{M}}^{o}}}(r_{\mathrm{S}})\, dr_{\mathrm{S}}. \quad (24)$$

By substituting (11), (12), (14) and (18) into (24), $P_{A_{\mathrm{M}}^{o}}^{\mathrm{UL}'}(\beta_{\mathrm{S}})$ can be obtained in (23), as shown at the bottom of this page.

IV. RESULTS AND DISCUSSION

In this section, we describe UL coverage probability results for ν while considering: (i) RFA and CA along with WBJs, and (ii) RFA and DeCA along with WBJs. The results are drawn from (22) and (23) using MATLAB 2017a. Moreover, (22) and (23) are validated through Monte Carlo simulations by using the simulation parameters listed in Table 2. MBSs, SBSs and users are considered to be distributed in $A_{\mathrm{M}} = \pi(1000\mathrm{m})^2$, s.t., $A_{\mathrm{M}} = A_{\mathrm{M}}^{c} \bigcap A_{\mathrm{M}}^{o}$. Similarly, WBJs are

TABLE 2. Simulation parameters.

Parameter	Configuration
Channel bandwidth	10 MHz
MBS and SBS distribution	IHPPP
WBJs distribution	MCP
Code iterations	1000
λ_{S}	$15 / \pi(1000\mathrm{m})^2$
λ_{M}	$3 / \pi(1000\mathrm{m})^2$
λ_J	$15 / \pi(100\mathrm{m})^2$
$P_{t,\mathrm{S}}^{\mathrm{DL}}$, $P_{t,\nu}^{\mathrm{UL}}$, $P_{t,J}$	30 dBm, 20 dBm and 10 dBm, respectively
$\alpha_m = \alpha_s = \alpha$	$2 < \alpha \leq 4$

$$P_{A_{\mathrm{M}}^{c}}^{\mathrm{UL}''}(\beta_{\mathrm{M}}) = \frac{2\pi\lambda_{\mathrm{M}}}{1-\exp(-\lambda_{\mathrm{M}}\pi d_1^2)} \int_{y}^{d_1} \exp\Bigg(\frac{\pi\beta_{\mathrm{M}} r_{\mathrm{M}}^{\alpha}}{\alpha/2-1}\Bigg[\lambda_{\mathrm{M}} d_1^{(2-\alpha)} \mathcal{J}\left(\alpha, -\beta_{\mathrm{M}}\left(\frac{r_{\mathrm{M}}}{d_1}\right)^{\alpha}\right) - \lambda_{\mathrm{M}} y^{(2-\alpha)} \mathcal{J}\left(\alpha, -\beta_{\mathrm{M}}\left(\frac{r_{\mathrm{M}}}{y}\right)^{\alpha}\right)$$
$$+\lambda_{\mathrm{S}}\eta_1\, x_2^{(2-\alpha)} \mathcal{J}\left(\alpha, -\beta_{\mathrm{M}}\eta_1\left(\frac{r_{\mathrm{M}}}{x_2}\right)^{\alpha}\right) - \lambda_{\mathrm{S}}\eta_1 x_1^{(2-\alpha)} \mathcal{J}\left(\alpha, -\beta_{\mathrm{M}}\eta_1\left(\frac{r_{\mathrm{M}}}{x_1}\right)^{\alpha}\right)\Bigg]$$
$$-\bar{c}\left[\left(\frac{2\mathrm{R}^{2+\alpha} r_{\mathrm{M}}^{-\alpha}}{\mathrm{R}^2(2+\alpha)\beta_{\mathrm{M}}\eta_2} \mathcal{J}\left(\alpha, -\left(\frac{\mathrm{R}^{\alpha}}{r_{\mathrm{M}}^{\alpha}\beta_{\mathrm{M}}\eta_2}\right)\right) - \frac{2z^{2+\alpha} r_{\mathrm{M}}^{-\alpha}}{\mathrm{z}^2(2+\alpha)\beta_{\mathrm{M}}\eta_2} \mathcal{J}\left(\alpha, -\left(\frac{z^{\alpha}}{r_{\mathrm{M}}^{\alpha}\beta_{\mathrm{M}}\eta_2}\right)\right)\right)\right] - \lambda_{\mathrm{M}}\pi r_{\mathrm{M}}^2\Bigg) r_{\mathrm{M}} dr_{\mathrm{M}}. \quad (21)$$

$$P_{A_{\mathrm{M}}^{o}}^{\mathrm{UL}''}(\beta_{\mathrm{M}}) = \frac{2\pi\lambda_{\mathrm{M}}}{\exp(-\lambda_{\mathrm{M}}\pi d_1^2)} \int_{d_1}^{d_2} \exp\Bigg(\frac{\pi\beta_{\mathrm{M}} r_{\mathrm{M}}^{\alpha}}{\alpha/2-1}\Bigg[\lambda_{\mathrm{M}} d_2^{(2-\alpha)} \mathcal{J}\left(\alpha, -\beta_{\mathrm{M}}\left(\frac{r_{\mathrm{M}}}{d_2}\right)^{\alpha}\right) - \lambda_{\mathrm{M}} d_1^{(2-\alpha)} \mathcal{J}\left(\alpha, -\beta_{\mathrm{M}}\left(\frac{r_{\mathrm{M}}}{d_1}\right)^{\alpha}\right)$$
$$+\lambda_{\mathrm{S}}\eta_1\, x_2^{(2-\alpha)} \mathcal{J}\left(\alpha, -\beta_{\mathrm{M}}\eta_1\left(\frac{r_{\mathrm{M}}}{x_2}\right)^{\alpha}\right) - \lambda_{\mathrm{S}}\eta_1 x_1^{(2-\alpha)} \mathcal{J}\left(\alpha, -\beta_{\mathrm{M}}\eta_1\left(\frac{r_{\mathrm{M}}}{x_1}\right)^{\alpha}\right)\Bigg]$$
$$-\bar{c}\left[\left(\frac{2\mathrm{R}^{2+\alpha} r_{\mathrm{M}}^{-\alpha}}{\mathrm{R}^2(2+\alpha)\beta_{\mathrm{M}}\eta_2} \mathcal{J}\left(\alpha, -\left(\frac{\mathrm{R}^{\alpha}}{r_{\mathrm{M}}^{\alpha}\beta_{\mathrm{M}}\eta_2}\right)\right) - \frac{2z^{2+\alpha} r_{\mathrm{M}}^{-\alpha}}{\mathrm{z}^2(2+\alpha)\beta_{\mathrm{M}}\eta_2} \mathcal{J}\left(\alpha, -\left(\frac{z^{\alpha}}{r_{\mathrm{M}}^{\alpha}\beta_{\mathrm{M}}\eta_2}\right)\right)\right)\right] - \lambda_{\mathrm{M}}\pi r_{\mathrm{M}}^2\Bigg) r_{\mathrm{M}} dr_{\mathrm{M}}. \quad (22)$$

$$P_{A_{\mathrm{M}}^{o}}^{\mathrm{UL}'}(\beta_{\mathrm{S}}) = \frac{2\pi\lambda_{\mathrm{S}}}{\exp(-\lambda_{\mathrm{M}}\pi d_1^2)} \int_{d_1}^{d_2} \exp\Bigg(\frac{\pi\lambda_{\mathrm{S}} r_{\mathrm{S}}^{\alpha}\beta_{\mathrm{S}}}{\alpha/2-1}\left(x_2^{(2-\alpha)}\eta_1 \mathcal{J}\left(\alpha, -\eta_1\beta_{\mathrm{S}}\left(\frac{r_{\mathrm{S}}}{x_2}\right)^{\alpha}\right) - x_1^{(2-\alpha)}\eta_1 \mathcal{J}\left(\alpha, -\eta_1\beta_{\mathrm{S}}\left(\frac{r_{\mathrm{S}}}{x_1}\right)^{\alpha}\right)\right.$$
$$+x_2^{(2-\alpha)} \mathcal{J}\left(\alpha, -\beta_{\mathrm{S}}\left(\frac{r_{\mathrm{S}}}{x_2}\right)^{\alpha}\right) - x_1^{(2-\alpha)} \mathcal{J}\left(\alpha, -\beta_{\mathrm{S}}\left(\frac{r_{\mathrm{S}}}{x_1}\right)^{\alpha}\right)\Bigg) - \lambda_{\mathrm{S}}\pi r_{\mathrm{S}}^2 - \bar{c}\left[\left(\frac{2\mathrm{R}^{2+\alpha} r_{\mathrm{S}}^{-\alpha}}{\mathrm{R}^2(2+\alpha)\beta_{\mathrm{S}}\eta_2}\right.\right.$$
$$\left.\left.\mathcal{J}\left(\alpha, -\left(\frac{\mathrm{R}^{\alpha}}{r_{\mathrm{S}}^{\alpha}\beta_{\mathrm{S}}\eta_2}\right)\right) - \frac{2z^{2+\alpha} r_{\mathrm{S}}^{-\alpha}}{\mathrm{z}^2(2+\alpha)\beta_{\mathrm{S}}\eta_2} \mathcal{J}\left(\alpha, -\left(\frac{z^{\alpha}}{r_{\mathrm{S}}^{\alpha}\beta_{\mathrm{S}}\eta_2}\right)\right)\right)\right]\Bigg) r_{\mathrm{S}} dr_{\mathrm{S}}. \quad (23)$$

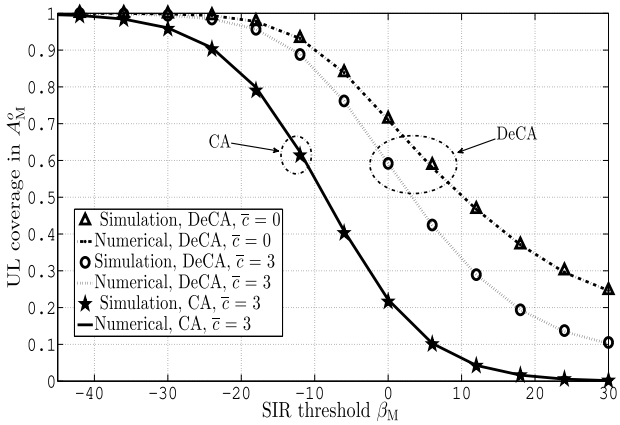

FIGURE 3. UL coverage in A_M^o versus SIR threshold β_M.

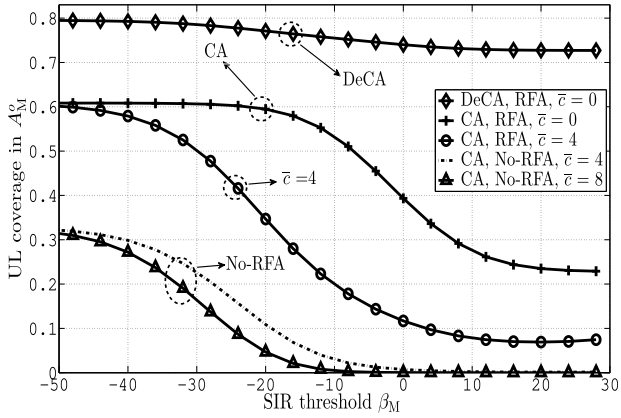

FIGURE 4. UL coverage in A_M^o versus SIR threshold β_M with effect of RFA versus no RFA.

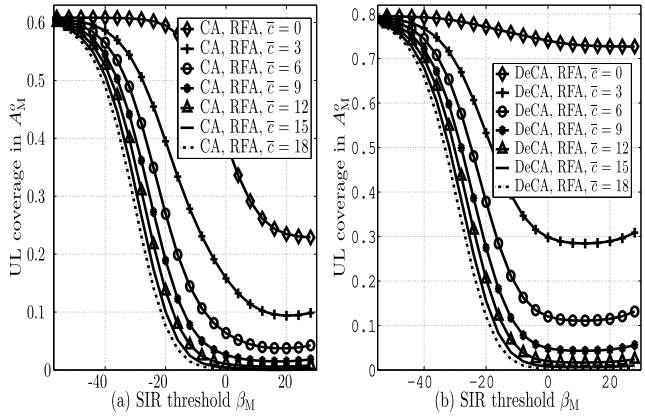

FIGURE 5. UL coverage in A_M^o versus SIR threshold β_M for (a) CA and (b) DeCA.

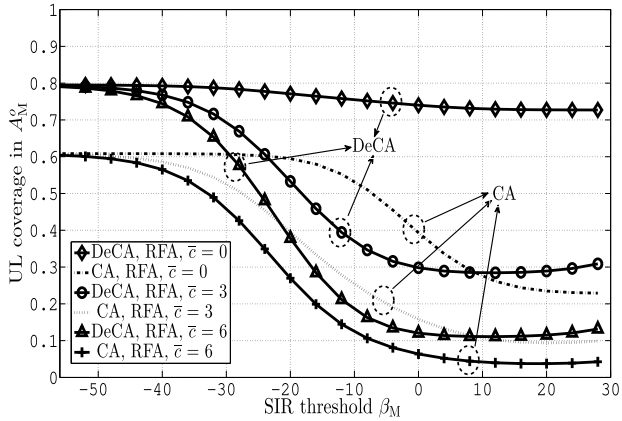

FIGURE 6. UL coverage in A_M^o versus SIR threshold β_M, with a comparison between CA and DeCA.

distributed in an area of $\pi(100\text{m})^2$ around ν. Moreover, MBS, SBS, ν, and WBJs transmit power are assumed to be 60 dBm, 40 dBm, 20dBm, and 10dBm, respectively. The effects of different network parameters, such as $P_{t,\nu}^{\text{UL}}$, λ_J, λ_M, λ_S, β_ν, and $P_{t,J}$ are considered for UL coverage while assuming that ν is located in A_M^o.

Fig. 3 presents the simulation and numerical results for UL coverage probabilities while using (22) and (23). The plots are generated for different values of β_M and $\bar{c}$ while assuming CA and DeCA. The results show that higher values of $\bar{c}$ lead to lower UL coverage due to higher JI. Moreover, DeCA with RFA outperform CA with RFA due to effective JI and ICI mitigation.

Fig. 4 compares UL coverage probabilities in A_M^o versus different values of SIR threshold β_M. The plots are generated by considering different plausible scenarios, such as with and without RFA, with and without DeCA, with CA, and with and without WBJs. The results signify that DeCA with RFA leads to improved coverage. It can be also observed that increasing $\bar{c}$ lowers the coverage probabilities in all the considered scenarios.

Figs. 5(a) and 5(b) compare UL coverage probabilities in A_M^o versus different values of SIR threshold β_M while assuming CA and DeCA, respectively. The plots are generated for $\bar{c} = 0$, 3, 6, 12, 15 and 18. Both the figures indicate that increasing $\bar{c}$ leads to lower coverage due to higher JI. Moreover, as compared with CA in Fig. 5(a), DeCA in Fig. 5(b) leads to improved coverage due to significant ICI mitigation.

Fig. 6 compares UL coverage probabilities in A_M^o versus different values of SIR threshold β_M while assuming CA and DeCA. The plots are generated for $\bar{c} = 0$, 3 an 6. The results show that DeCA outperforms CA for different values of $\bar{c}$. Moreover, an increase in the value of $\bar{c}$ leads to lower coverage. This is due to higher $\bar{c}$, which leads to increased JI.

Figs. 7(a) and 7(b) compare UL coverage probabilities in A_M^o versus different values of $P_{t,\nu}^{\text{UL}}$, while assuming CA and DeCA, respectively. The result is generated for $\beta_M = 50$ dB and $\bar{c} = 4$, 8, 12, 16 and 20. The result demonstrates that increasing the values of $\bar{c}$ lowers the coverage due to higher JI. Moreover, it is observed from the figure that DeCA promptly improves the coverage as compared with CA due to improved UL SIR.

Figs. 8(a) and 8(b) compare UL coverage probabilities in A_M^o versus different values of $P_{t,J}$, while assuming CA and DeCA, respectively. Both the figures are generated for $\beta_M = 50$ dB and $\bar{c} = 4$, 8, 12, 16 and 20. The figures depict that higher values of $P_{t,J}$ cause lower coverage due to severe JI. Similarly, Fig. 9 shows UL coverage improvement due to

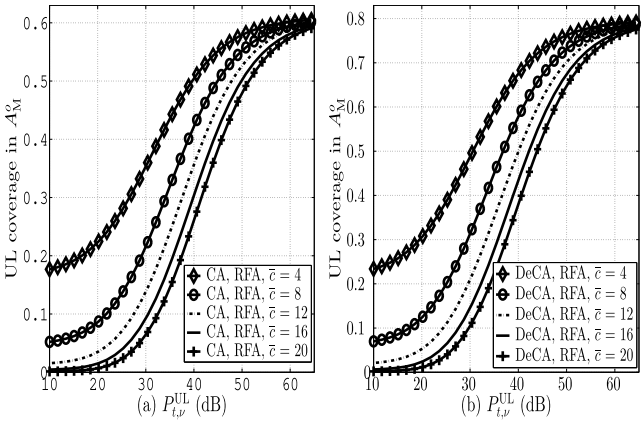

FIGURE 7. UL coverage in A_M^o versus $P_{t,\nu}^{UL}$ for (a) CA and (b) DeCA.

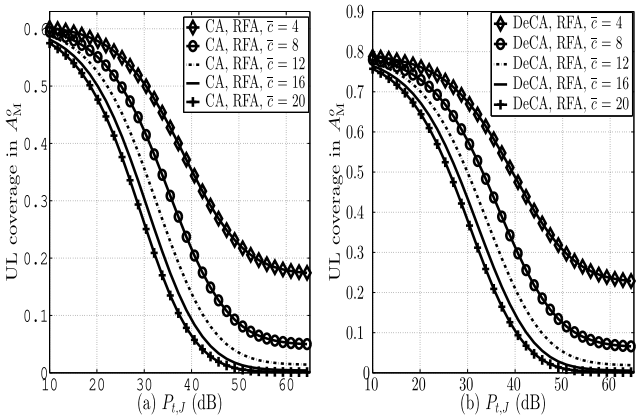

FIGURE 8. UL coverage in A_M^o versus $P_{t,J}$ for (a) CA and (b) DeCA.

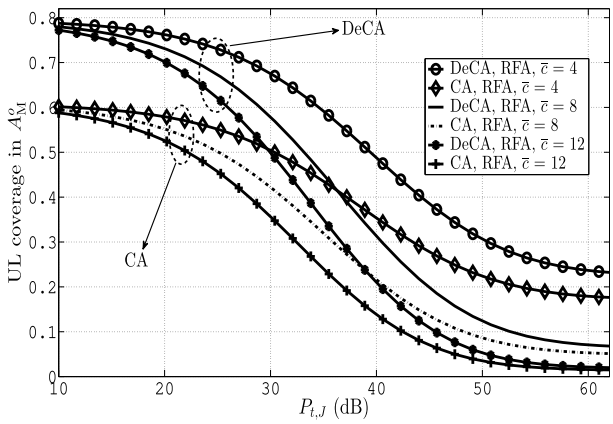

FIGURE 9. UL coverage in A_M^o versus $P_{t,J}$ for CA and DeCA.

DeCA as compared with CA for the same set of parameters as of Figs. 8(a) and 8(b). Moreover, Fig. 9 shows that the higher values of $\bar{c}$ lower the UL coverage due to significant JI.

Fig. 10 presents UL coverage in A_M^o versus different values of jammers' cluster radius (R) for CA and DeCA. The figure shows that as the value of R increases, the UL coverage also increases. This is because WBJs are now distributed

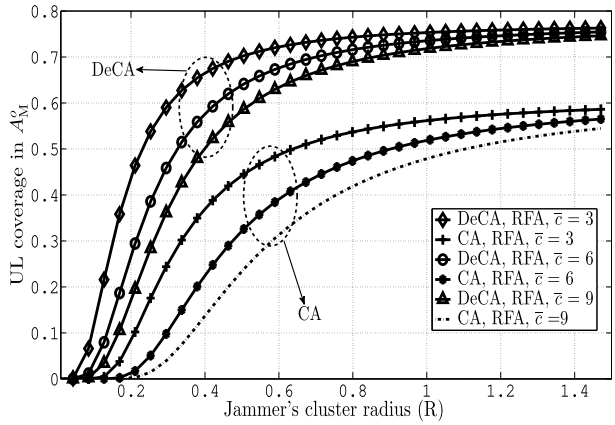

FIGURE 10. UL coverage in A_M^o versus jammer's cluster radius (R) for CA and DeCA.

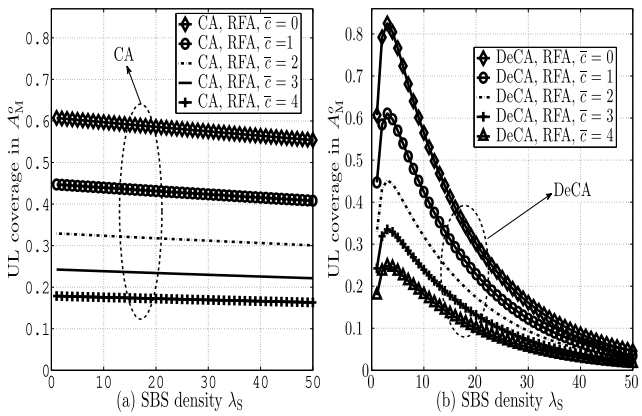

FIGURE 11. UL coverage in A_M^o versus different values of λ_S for (a) CA and (b) DeCA.

in a larger area and, thus, lead to reduce JI. Moreover, the result also shows that DeCA leads to better UL coverage as compared with CA for all values of $\bar{c}$ because of improved ICI mitigation.

Figs. 11(a) and 11(b) compare UL coverage probabilities in A_M^o versus different values of SBS density λ_S, while assuming CA and DeCA, respectively. Both the figures are generated for $\beta_M = 50$ dB, $\bar{c} = 0, 1, 2, 3$ and 4, and $\lambda_S = 0$ to 50. In Fig. 11(b), UL coverage decreases with increase in the value of λ_S due to the fact that ν associates with SBS following DeCA. However, in 11(a), UL coverage remains unchanged against increase in the value of λ_S due to the fact that ν is associated with MBS by following CA. Moreover, both the figures depict decrease in the UL coverage by increasing the values of $\bar{c}$ due to higher JI.

V. CONCLUSION

In HetNets with CA, ICI is one of the main limiting performance factors. The situation exacerbates if there exist intentional jammers. In this paper, we investigate clustered WBJs attacks, where the WBJs are placed around the target in close proximity. The results are generated by investigating different

network parameters, such as SINR threshold, jammers' transmit power and density, SBS density, typical user UL transmit power, and radius of jammers' cluster. The results indicate that the UL coverage is significantly reduced by increase in WBJs' density and transmit power. As a countermeasure to both ICI and JI, we use DeCA in conjunction with RFA. The results show considerable UL coverage improvement by using DeCA with RFA as opposed to CA with RFA.

APPENDIX

PROOF OF STEP (2) AS OBTAINED FROM STEP (1) IN (8)

Proof : From [2], [27], we obtain $P^{\mathrm{UL}''}_{A^c_{\mathrm{M}}}(\beta_{\mathrm{M}})$ as

$$P^{\mathrm{UL}''}_{A^c_{\mathrm{M}}}(\beta_{\mathrm{M}}) = P\left(\frac{P^{\mathrm{UL}}_{t,\nu}|h_{\mathrm{M}}|r_{\mathrm{M}}^{-\alpha}}{I^{\mathrm{UL}}_{\phi_{\mathrm{M}},A^c_{\mathrm{M}}} + I^{\mathrm{DL}}_{\phi_{\mathrm{S}},A^o_{\mathrm{M}}} + I_{\phi_J,A^o_{\mathrm{M}}}} > \beta_{\mathrm{M}}\right). \quad (25)$$

By keeping $|h_{\mathrm{M}}|$ on one side of the inequality and moving the rest of the parameters to the other side, we transform (25) as

$$P^{\mathrm{UL}''}_{A^c_{\mathrm{M}}}(\beta_{\mathrm{M}}) = P\left(|h_{\mathrm{M}}| > \frac{r_{\mathrm{M}}^{\alpha}\beta_{\mathrm{M}}}{P^{\mathrm{UL}}_{t,\nu}}\left(I^{\mathrm{UL}}_{\phi_{\mathrm{M}},A^c_{\mathrm{M}}} + I^{\mathrm{DL}}_{\phi_{\mathrm{S}},A^o_{\mathrm{M}}} + I_{\phi_J,A^o_{\mathrm{M}}}\right)\right). \quad (26)$$

Now, using (2.11) of [27], (26) transforms into the expression of Step (2) in (8).

REFERENCES

[1] M. A. Klatt, J. Lovrić, D. Chen, S. C. Kapfer, F. M. Schaller, P. W. Schönhöfer, B. S. Gardiner, A.-S. Smith, G. E. Schröder-Turk, and S. Torquato, "Universal hidden order in amorphous cellular geometries," *Nat. Commun.*, vol. 10, no. 1, p. 811, 2019.

[2] Z. H. Abbas, F. Muhammad, and L. Jiao, "Analysis of load balancing and interference management in heterogeneous cellular networks," *IEEE Access*, vol. 5, p. 14690–14705, 2017.

[3] M. S. Haroon, Z. H. Abbas, F. Muhammad, and G. Abbas, "Coverage analysis of cell-edge users in heterogeneous wireless networks using Stienen's model and RFA scheme," *Int. J. Commun. Syst.*, p. e4147, Sep. 2019.

[4] M. S. Haroon, Z. H. Abbas, G. Abbas, and F. Muhammad, "Analysis of interference mitigation in heterogeneous cellular networks using soft frequency reuse and load balancing," in *Proc. 28th Int. Telecommun. Netw. Appl. Conf. (ITNAC)*, Nov. 2018, pp. 1–6.

[5] R. P. Jover, "Security attacks against the availability of LTE mobility networks: Overview and research directions," in *Proc. 16th Int. Symp. Wireless Pers. Multimedia Commun. (WPMC)*, Jun. 2013, pp. 1–9.

[6] Y. Huo, X. Fan, L. Ma, X. Cheng, Z. Tian, and D. Chen, "Secure communications in tiered 5G wireless networks with cooperative jamming," *IEEE Trans. Wireless Commun.*, vol. 18, no. 6, pp. 3265–3280, Jun. 2019.

[7] W. Jundong, "Complex environment noise barrage jamming effects on airborne warning radar," *Amer. J. Remote Sens.*, vol. 6, no. 2, pp. 59–63, 2018.

[8] A. Viterbi, "A robust ratio-threshold technique to mitigate tone and partial band jamming in coded mfsk systems," in *Proc. IEEE Military Commun. Conf.-Prog. Spread Spectr. Commun.*, vol. 1, Oct. 1982, pp. 22.4-1–22.4-5.

[9] M. S. Haroon, S. Ahmad, and J. A. Khan, "LLR-based erasure decoding of SFH-MFSK in the presence of tone jamming," in *Proc. 11th Int. Bhurban Conf. Appl. Sci. Technol. (IBCAST)*, Jan. 2014, pp. 453–457.

[10] C. V. Ham and T. E. Scoughton, "Radio frequency jammer," U.S. Patent 7 318 368, Jan. 15, 2008.

[11] K. Grover, A. Lim, and Q. Yang, "Jamming and anti-jamming techniques in wireless networks: A survey," *Int. J. Ad Hoc Ubiquitous Comput.*, vol. 17, no. 4, pp. 197–215, 2014.

[12] S. Wang, Y. Gao, N. Sha, G. Zhang, and G. Zang, "Physical layer security in k-tier heterogeneous cellular networks over nakagami-m channel during uplink and downlink phases," *IEEE Access*, vol. 7, pp. 14581–14592, 2019.

[13] J. G. Andrews, S. Buzzi, W. Choi, S. V. Hanly, A. Lozano, A. C. K. Soong, and J. C. Zhang, "What will 5G be?" *IEEE J. Sel. Areas Commun.*, vol. 32, no. 6, pp. 1065–1082, Jun. 2014.

[14] S. Sekander, H. Tabassum, and E. Hossain, "Decoupled uplink-downlink user association in multi-tier full-duplex cellular networks: A two-sided matching game," *IEEE Trans. Mobile Comput.*, vol. 16, no. 10, pp. 2778–2791, Oct. 2017.

[15] N. Naganuma, S. Nakazawa, S. Suyama, Y. Okumura, and H. Otsuka, "Performance evaluation of adaptive control CRE in HetNet with EICIC scheme," *IEICE Commun. Express*, vol. 6, no. 4, pp. 166–171, 2017.

[16] M. Fereydooni, M. Sabaei, M. Dehghan, G. B. Eslamlou, and M. Rupp, "Analytical evaluation of heterogeneous cellular networks under flexible user association and frequency reuse," *Comput. Commun.*, vol. 116, pp. 147–158, Jan. 2018.

[17] L. Guo, S. Cong, and Z. Sun, "Multichannel analysis of soft frequency reuse and user association in two-tier heterogeneous cellular networks," *EURASIP J. Wireless Commun. Netw.*, vol. 2017, no. 1, p. 168, Oct. 2017.

[18] M. Lichtman, J. D. Poston, S. Amuru, C. Shahriar, T. C. Clancy, R. M. Buehrer, and J. H. Reed, "A communications jamming taxonomy," *IEEE Security Privacy*, vol. 14, no. 1, pp. 47–54, Jan./Feb. 2016.

[19] S. Gecgel, C. Goztepe, and G. K. Kurt, "Jammer detection based on artificial neural networks: A measurement study," in *Proc. ACM Workshop Wireless Secur. Mach. Learn.*, 2019, pp. 43–48.

[20] L. Zhang, F. Restuccia, T. Melodia, and S. M. Pudleswki, "Jam sessions: Analysis and experimental evaluation of advanced jamming attacks in MIMO networks," Apr. 2019, *arXiv:1904.07613*. [Online]. Available: https://arxiv.org/abs/1904.07613

[21] M. N. Sial and J. Ahmed, "A realistic uplink–downlink coupled and decoupled user association technique for k-tier 5G HetNets," *Arabian J. for Sci. Eng.*, vol. 44, no. 3, pp. 2185–2204, 2019.

[22] F. Muhammad, Z. H. Abbas, G. Abbas, and L. Jiao, "Decoupled downlink-uplink coverage analysis with interference management for enriched heterogeneous cellular networks," *IEEE Access*, vol. 4, pp. 6250–6260, 2016.

[23] M. Arif, S. Wyne, and J. Ahmed, "Performance analysis of downlink and uplink decoupled access in clustered heterogeneous cellular networks," *Telecommun. Syst.*, vol. 72, pp. 355–364, Apr. 2019.

[24] F. Muhammad, Z. H. Abbas, and F. Y. Li, "Cell association with load balancing in nonuniform heterogeneous cellular networks: Coverage probability and rate analysis," *IEEE Trans. Veh. Technol.*, vol. 66, no. 6, pp. 5241–5255, Jun. 2017.

[25] M. S. Haroon, Z. H. Abbas, G. Abbas, and F. Muhammad, "Coverage analysis of ultra-dense heterogeneous cellular networks with interference management," *Wireless Netw.*, to be published, doi: 10.1007/s11276-019-01965-0.

[26] A. Ijaz, S. A. Hassan, S. A. R. Zaidi, D. N. K. Jayakody, and S. M. H. Zaidi, "Coverage and rate analysis for downlink HetNets using modified reverse frequency allocation scheme," *IEEE Access*, vol. 5, pp. 2489–2502, 2017.

[27] B. Błaszczyszyn, M. Haenggi, P. Keeler, and S. Mukherjee, *Stochastic Geometry Analysis of Cellular Networks*. Cambridge, U.K.: Cambridge Univ. Press, 2018.

[28] C. Dai, K. Zhu, R. Wang, and Y. Xu, "Decoupled multiple association in full-duplex ultra-dense networks: An evolutionary game approach," in *Proc. Int. Conf. Commun. (ICC)*, May 2019, pp. 1–6.

[29] H. Munir, S. A. Hassan, H. Pervaiz, Q. Ni, and L. Musavian, "User association in 5G heterogeneous networks exploiting multi-slope path loss model," in *Proc. 2nd Workshop Recent Trends Telecommun. Res. (RTTR)*, Feb. 2017, pp. 1–5.

[30] X. Zhang and J. G. Andrews, "Downlink cellular network analysis with multi-slope path loss models," *IEEE Trans. Commun.*, vol. 63, no. 5, pp. 1881–1894, May 2015.

[31] C. Saha, M. Afshang, and H. S. Dhillon, "3GPP-inspired HetNet model using Poisson cluster process: Sum-product functionals and downlink coverage," *IEEE Trans. Commun.*, vol. 66, no. 5, pp. 2219–2234, May 2018.

[32] M. Afshang, C. Saha, and H. S. Dhillon, "Nearest-neighbor and contact distance distributions for Matérn cluster process," *IEEE Commun. Lett.*, vol. 21, no. 12, pp. 2686–2689, Dec. 2017.

[33] R. Hernandez-Aquino, S. A. R. Zaidi, D. McLernon, and M. Ghogho, "Modelling and performance evaluation of non-uniform two-tier cellular networks through Stienen model," in *Proc. Int. Conf. Commun. (ICC)*, May 2016, pp. 1–6.
[34] H. Tabassum, E. Hossain, and J. Hossain, "Modeling and analysis of uplink non-orthogonal multiple access in large-scale cellular networks using Poisson cluster processes," *IEEE Trans. Commun.*, vol. 65, no. 8, pp. 3555–3570, Aug. 2017.
[35] N. Deng, W. Zhou, and M. Haenggi, "Outage and capacity of heterogeneous cellular networks with intra-tier dependence," in *Proc. 6th Int. Conf. Wireless Commun. Signal Process. (WCSP)*, Oct. 2014, pp. 1–5.

FAZAL MUHAMMAD received the B.Sc. and M.Sc. degrees in electrical engineering from the University of Engineering and Technology, Peshawar, Pakistan, in 2004 and 2007, respectively, and the Ph.D. degree in electronic engineering from the GIK Institute of Engineering Sciences and Technology, Pakistan, in 2017. He is currently working as an Assistant Professor and the Head of Electrical Engineering Department, City University of Sciences and Information Technology, Peshawar. He is also the Secretary of Institutions of Engineers, Pakistan, Peshawar Center. His research interests include heterogeneous cellular networks, cognitive radio networks, and optical networks.

MUHAMMAD SAJID HAROON received the B.Sc. degree in electronics engineering from the International Islamic University Islamabad, Pakistan, in 2007, and the M.S. degree in electrical engineering from the COMSATS Institute of Information Technology, Attock, Pakistan, in 2013. He is currently pursuing the Ph.D. degree with the Ghulam Ishaq Khan Institute of Engineering Science and Technology, Swabi, Pakistan, with a focus on interference management in next generation cellular networks using tools from stochastic geometry, point process theory, and spatial statistics. His research interests include interference mitigation in cellular networks, next generation cellular networks, stochastic processes, and digital signal processing.

ZIAUL HAQ ABBAS received the M.Phil. degree in electronics from the Quaid-e-Azam University, Pakistan, in 2001, and the Ph.D. degree from the Agder Mobility Laboratory, Department of Information and Communication Technology, University of Agder, Norway, in 2012. In 2012, he was a Visiting Researcher with the Department of Electrical and Computer Engineering, University of Minnesota, USA. He is currently an Associate Professor with the Faculty of Electrical Engineering and a Co-Founding Member of the Telecommunications and Networking (TeleCoN) Research Lab, GIK Institute. His research interests include energy efficiency in hybrid mobile and wireless communications networks, 4G and beyond mobile systems, mesh and ad hoc networks, traffic engineering in wireless networks, performance evaluation of communications protocols and networks by analysis and simulation, quality-of-service in wireless networks, green wireless communications, and cognitive radio.

GHULAM ABBAS received the B.S. degree in computer science from the University of Peshawar, Pakistan, in 2003, and the M.S. degree in distributed systems and the Ph.D. degree in computer networks from the University of Liverpool, U.K., in 2005 and 2010, respectively. From 2006 to 2010, he was a Research Associate with Liverpool Hope University, U.K., where he was associated with the Intelligent and Distributed Systems Laboratory. Since 2011, he has been with the Faculty of Computer Sciences and Engineering, GIK Institute of Engineering Sciences and Technology, Pakistan. He is currently working as an Associate Professor and the Director of Huawei Network Academy. He is also a Co-Founding Member of the Telecommunications and Networking (TeleCoN) Research Lab, GIK Institute. He is also a Fellow of the Institute of Science and Technology, U.K., and the British Computer Society. His research interests include computer networks and wireless and mobile communications.

SUNGHWAN KIM received the B.S., M.S., and Ph.D. degrees from Seoul National University, South Korea, in 1999, 2001, and 2005, respectively. He was a Postdoctoral Visitor with the Georgia Institute of Technology (GeorgiaTech), from 2005 to 2007 and a Senior Engineer with Samsung Electronics, from 2007 to 2011. He is currently a Professor with the School of Electrical Engineering, University of Ulsan, South Korea. His main research interests are channel coding, modulation, massive MIMO, visible light communication, and quantum information.